ARL-TN-1130 ● AUG 2022

DEVCOM ARMY RESEARCH LABORATORY

Non-Beam Additive Manufacturing of Metals

by Kazzandra Alaniz, Risheil Ortiz Ayala, Zachary Theimer, Devyn White, Gregory Wong, Brady G Butler, and James D Paramore

NOTICES

Disclaimers

The findings in this report are not to be construed as an official Department of the Army position unless so designated by other authorized documents.

Citation of manufacturer's or trade names does not constitute an official endorsement or approval of the use thereof.

Destroy this report when it is no longer needed. Do not return it to the originator.

ARL-TN-1130 ● AUG 2022

Non-Beam Additive Manufacturing of Metals

Brady G Butler and James D Paramore
DEVCOM Army Research Laboratory

Kazzandra Alaniz, Risheil Ortiz Ayala, Zachary Theimer, Devyn White, and Gregory Wong
Texas A&M University, Department of Materials Science and Engineering
Capstone Team 7

REPORT DOCUMENTATION PAGE

Form Approved
OMB No. 0704-0188

1. REPORT DATE *(DD-MM-YYYY)*	2. REPORT TYPE	3. DATES COVERED (From - To)
August 2022	Technical Note	August 2020–May 2021

4. TITLE AND SUBTITLE
Non-Beam Additive Manufacturing of Metals

5a. CONTRACT NUMBER

5b. GRANT NUMBER

5c. PROGRAM ELEMENT NUMBER

6. AUTHOR(S)
Kazzandra Alaniz, Risheil Ortiz Ayala, Zachary Theimer, Devyn White, Gregory Wong, Brady G Butler, and James D Paramore

5d. PROJECT NUMBER
W911NF-19-2-0264

5e. TASK NUMBER

5f. WORK UNIT NUMBER

7. PERFORMING ORGANIZATION NAME(S) AND ADDRESS(ES)
DEVCOM Army Research Laboratory
ATTN: FCDD-RLW-MF
Aberdeen Proving Ground, MD 21005

8. PERFORMING ORGANIZATION REPORT NUMBER
ARL-TN-1130

9. SPONSORING/MONITORING AGENCY NAME(S) AND ADDRESS(ES)

10. SPONSOR/MONITOR'S ACRONYM(S)

11. SPONSOR/MONITOR'S REPORT NUMBER(S)

12. DISTRIBUTION/AVAILABILITY STATEMENT
Approved for public release: distribution unlimited.

13. SUPPLEMENTARY NOTES
ORCID IDs: Brady Butler, 0000-0002-7677-9685; James Paramore, 0000-0001-8058-7662

14. ABSTRACT
Additive manufacturing of titanium alloys has significant potential as a disruptive technology. While conventional additive manufacturing routes use electron or laser beams to selectively melt materials into the final component geometry, alternative non-beam-based methods show the strongest potential for reducing cost and improving throughput of additive manufacturing technologies. This research focuses on a Capstone senior design program to evaluate two non-beam-based additive manufacturing methods: binder jetting and metal extrusion. The results of sintering and thermohydrogen treatments on a titanium alloy (Ti-6Al-4V) are assessed in terms of the mechanical and microstructural characterization.

15. SUBJECT TERMS
Science of Extreme Materials, titanium alloys, additive manufacturing, binder jetting, metal extrusion, thermohydrogen refinement of microstructure, hydrogen sintering

16. SECURITY CLASSIFICATION OF:			17. LIMITATION OF ABSTRACT	18. NUMBER OF PAGES	19a. NAME OF RESPONSIBLE PERSON
a. REPORT	b. ABSTRACT	c. THIS PAGE			Brady Butler
Unclassified	Unclassified	Unclassified	UU	29	19b. TELEPHONE NUMBER (Include area code) (410) 306-0835

Contents

List of Figures

List of Tables

Acknowledgments

This project was supported through a Cooperative Agreement between the US Army Combat Capabilities Development Command Army Research Laboratory and Texas A&M University under contract number W911NF-19-2-0264.

The team would like to express its sincerest appreciation to its industrial mentors, Dr Brady Butler and Dr James Paramore of the DEVCOM Army Research Laboratory at Texas A&M University and its staff for granting the team access to the DEVCOM ARL facilities, providing the team with required materials, and guiding the team in this research. Without their support, this project would not have been possible, and the individuals on the team would not have had this opportunity to develop themselves as engineers and scientists.

The team would also like to thank Dr Abhinav Srivastava and Griffin Turner for supervising lab work and teaching in the research process. Their enthusiasm and experience proved to be crucial to this project.

Also, thank you to Daniel Lewis for providing a technical review of this manuscript.

Lastly, the team would like to give a special thanks to Dr Homero Castaneda-Lopez for leading our Capstone lecture.

Executive Summary

This report describes the process by which Capstone Team 7 of Texas A&M University's Department of Materials Science and Engineering tested a procedure to additively manufacture Ti-6Al-4V parts using non-beam-based methods. This began by understanding two of the most common non-beam metallic additive manufacturing processes: metal extrusion additive manufacturing (MEAM) and binder jet additive manufacturing. Following this, the team devised a strategy to test parts for mechanical strength, ductility, and density using a combination of tensile testing, hardness testing, Archimedes density measurements, and scanning electron microscopy with the goal of satisfying standard AMS4999[*] and producing Ti-6Al-4V components with equivalent properties to products fabricated by metal deposition.

Experiments concluded that binder jetting, followed by direct sintering in a hydrogen atmosphere, left too many intrinsic pores to be viable without further process development. An alternative process, MEAM, followed by conventional sintering and thermohydrogen refinement of microstructure (THRM), resulted in a viable manufacturing process, which satisfied the majority of the property metrics outlined in the standard. This sintering method utilizes hydrogen as a temporary alloy addition, allowing for phase transformations in the material that refine larger grains of the bulk sintered component into smaller grains. The refined titanium (Ti) alloy is dehydrogenated under vacuum at moderate temperatures. Finally, conventional Ti heat treatments are used to globularize and age the microstructure. In combination with THRM, this creates an additively manufactured part with a microstructure comparable to wrought material.

Finally, the team suggested that further study could be performed to understand the relationship between powder feedstock properties and the density of the parts, as well as further optimize the sintering parameters. These steps have a strong potential for improving the mechanical properties of the parts, ensuring higher consistency in surpassing the requirements of AMS4999.

[*] AMS4999A. Titanium alloy direct deposited products 6Al - 4V annealed. SAE International; 2016 Sep 26.

1. Introduction

This report describes the process by which Capstone Team 7 of Texas A&M University's Department of Materials Science and Engineering tested a procedure to additively manufacture Ti-6Al-4V parts using non-beam-based methods with the goal of satisfying standard AMS4999[1] and producing Ti-6Al-4V components with equivalent properties to products fabricated by metal deposition.

2. Background

The most common metallic additive manufacturing (AM) processes are beam-based methods such as selective laser melting (SLM) and electron beam melting. However, these methods have many limitations and beamless methods are currently under investigation by many researchers around the world. Non-beam metallic AM is a fairly new method that is under development.

Despite the popularity of laser and electron beam-based methods for metal AM, these processes are heavily restrictive due to both material and process limitations, which affect the reliability of the final products and limit production on an industrial scale. In addition to low build rates and demanding feedstock requirements for beam-based methods, many issues are caused by the intense local thermal effects of the electron or laser beam on the metal surface. The thermal process history is inherently difficult to control and can vary widely in a single printed component. This can lead to poor mechanical properties, cracking, and porosity. It also severely limits the ability to process complex metals with a fine-tuned microstructure, such as precipitation-hardened alloys, where temperature and other processing parameters must be uniformly controlled. Additionally, this process has historically required a significantly high material and labor cost, including highly trained operators and a very narrow particle size distribution of metal powders. Given these restrictions, AM researchers are investigating novel non-beam AM methods that can process a wider range of materials at a lower cost and with higher rates of production.[2]

Non-beam metal AM has various processes that may be used, yet there are two that are considered to be the most prevalent: binder jetting and metal extrusion.[3] Since 2012, there has been a continuous growth in the number of industries that have started to use non-beam metal AM.[3] In non-beam AM, metallic powders are fused together without the use of a laser or electron beam. Instead, these processes form a green (i.e., an unsintered, near-net-shape part composed of bound metal powder) component by printing layer by layer. This part is then sintered using more conventional heating sources to sinter the metallic powders in a separate processing

step. Through this method, residual stress is minimized as the green parts are sintered after printing.[3]

Binder jetting additive manufacturing (BJAM) is a layer-by-layer additive process,[2] as shown in the schematic of Fig. 1. A roller is used to move the powder from the feedstock container into the build area. Pistons move the feedstock up and the build platform down to accommodate this flow of powder and create a constant layer thickness. Binder jetting utilizes an inkjet printhead, which allows for the powder to be fused in the XY-direction by being surface sprayed with a binder. This binder also penetrates between layers and allows for fusion in the Z-direction. The curing stage is completed within the build box, which is implemented because of added rigidity from the polymer binder.[4] Thermal debinding then removes the polymer binding agent, and the sintering process finishes the densification process and bonds the metal. The advantage of binder jetting is that the inkjet printhead improves the speed of printing, and the process allows for multiple layers of parts to be built simultaneously.

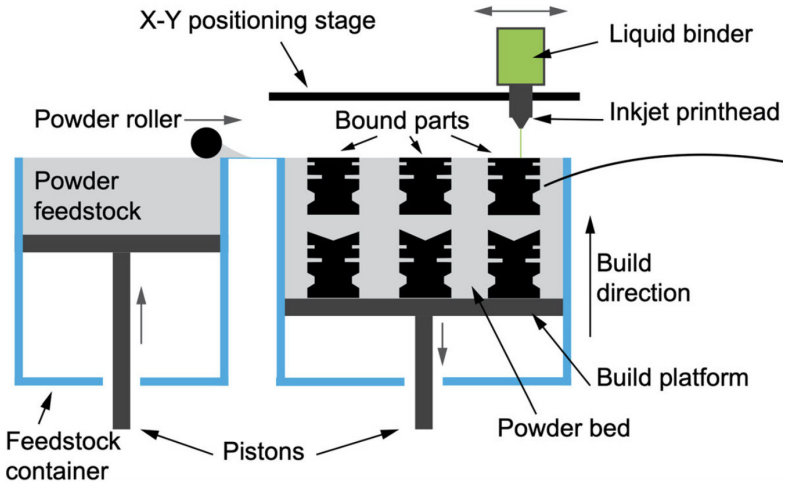

Fig. 1 Binder jetting process[2]

In a study performed by the mechanical engineering department of the University of Pittsburgh, the effect of the powder particle size distribution in binder jetting was investigated. When it comes to fine and coarse powders with a narrow particle size distribution, there are complications that can be caused by binder jetting.[5] The complications it may cause involve many pores being created, which decreases the overall density of the metal significantly. The metallic particles are not able to fully pack during the final sintering process.[5] Therefore, it was discovered that particle size is a parameter that must be taken into consideration when using BJAM so that pore sizes can be minimized and the final microstructure can be dense and closely packed together.

Research performed by Bai and Williams used a particle-free metal ink called metal–organic decomposition as the binding agent for binder jetting to create a final metallic product. As the ink is heated, metallic nanoparticles are formed that can strongly bond to one another when being deposited onto the bed.[6] The nanoparticles can then be fused together through sintering. The final product is then a solidified metal that is very dense in the middle, but its outer shell is porous, mostly due to weak bonding at the surface.[6] Overall, it was found that this method is effective because of its lower cost and its ability to alleviate some of the problems with particle suspension.[6]

Ziaee, Tridas, and Crane created stainless steels through fine powder agglomerates and nylon12 powder mixed with the stainless steel. Their work resulted in final products with variations in density due to the different parameters that were used.[7] Because binder jetting uses sintering to fuse the metallic particles together, sintering is a huge part of the AM. Ziaee and colleagues found that the sintering density can be reduced by both methods: fine particle agglomerates and a mixture with nylon12. Therefore, if changes are applied to the sintering process for binder jetting, then there can result in a closer value to 100% density of the material, which is the goal.[7]

Metal extrusion additive manufacturing (MEAM) was created in 1989 by Stratasys.[2,8] In metal extrusion, metallic powders are mixed with organic binders to create the feedstock, which is the material that creates the overall structure being printed. The feedstock is heated up to its melting point and is extruded through a nozzle so that it may be deposited layer by layer onto a platform. The nozzle depositing the feedstock moves vertically, while the platform moves horizontally so that a 3-D structure can be built. When the part is finished being built, it must be debound using solvent, catalytic, or thermal debinding methods before being sent to a sintering furnace so that the metal particles can be fused together.[2,8] Because metal extrusion is a non-beam AM process, a laser or electron source is not needed to be able to 3-D print a metallic material. Therefore, this lowers the production cost significantly as energy-based sources are generally cheaper.[3]

In a study done by Gong et al., the differences between non-beam and beam-based AM were studied on stainless steel 316L. Mechanical testing such as hardness, tensile strength, and microstructure analysis was performed on the material. It was found that metal extrusion had slightly smaller values for the performed testing. However, metal extrusion was also deemed the best option to use because of its low cost and easy use.[9] This study reveals that MEAM is a lot less cost prohibitive than SLM.

In another study performed by Annoni and colleagues, a new metal extrusion process was proposed with high-viscosity mixtures and low polymer accumulation (Fig 2).[10] Binder percentage and the nozzle diameter were tested during this research to see their effects on extrudability and cohesion of the printed material. It was found that a nozzle with a diameter of 0.9 mm was ideal for this process. It was also found that each material has to have an optimal binder percentage because a higher binder percentage may improve bonding but may make it harder to remove the binder prior to sintering. This means that the sample will have a relatively high amount of polymer left in it, which is not ideal for material performance after sintering. This study found that the new metal extrusion process resulted in a high density, indicating that the porosity was at a minimum.[10]

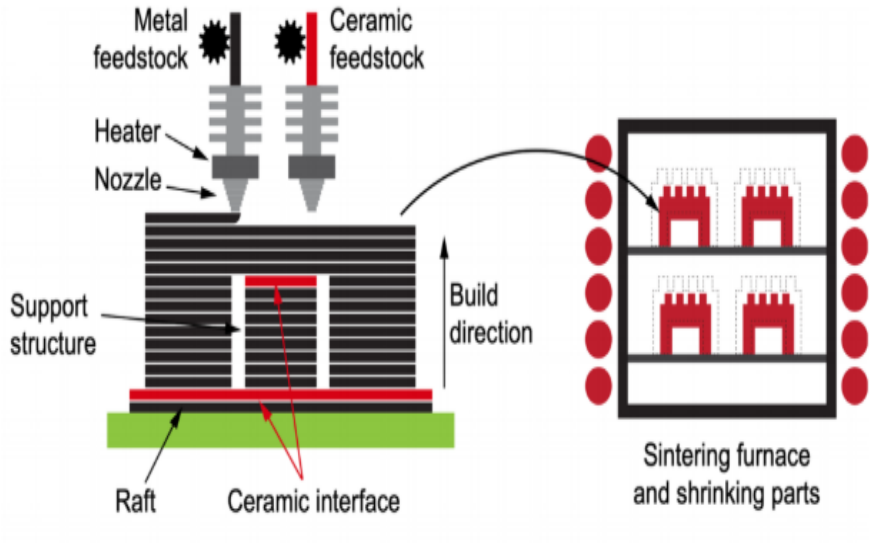

Fig. 2 Metal extrusion process in non-beam AM[8]

Non-beam AM typically creates stronger and more uniform microstructures than beam-based AM, because it relies on uniform sintering to decrease porosity in the structure. Beam-based AM uses a laser to melt a powder before allowing it to resolidify. This change in state causes nonuniform microstructure throughout the material and provides poor mechanical properties as well. On the other hand, non-beam AM uses sintering to form the structure without a change of state. Sintering is thermodynamically driven by the minimization of surface energy, which promotes bonding between particles. A low porosity can be achieved by high temperature and long sintering times.[11]

Hydrogen sintering and phase transformation (HSPT) is a novel process where titanium (Ti) alloys are sintered in a hydrogen atmosphere to promote densification, while special phase transformations are subsequently used to refine the microstructure. This process can be closely related to the thermohydrogen

refinement of microstructure (THRM) process, which is utilized to refine the microstructure of bulk components. Considering that the printer originally used was unavailable, the group decided to go through a powder metallurgy process to mimic non-beam AM. Therefore, HSPT was one of the processes studied, as well as vacuum sintering (VS), another popular process within powder metallurgy and AM.

HSPT is a sintering-based powder metallurgy process that uses hydrogen during the sintering process to achieve an ultra-refined microstructure.[12] In a study done by Sun et al.,[12] the group focused on the HSPT process on Ti-6Al-4V because pre-alloy Ti was deemed to have a very coarse microstructure through conventional VS; therefore, the project aimed to understand what role HSPT could have in the microstructure of Ti.[12] They found that HSPT created the ultra-refined microstructure through precipitation of the fine α/α_2 particles within the β grains and the eutectoid transformation of the remaining β grains into fine grains at low temperatures.[12]

VS is one of the more common processing methods in powder metallurgy and AM. In this process, a vacuum atmosphere is used to allow the material to minimize its pores and become denser. However, it has been discovered that this method often does not lead to a minimum of 98% densification, which is the goal.[13] A study done by Luo and colleagues examined the densification of Ti in an argon atmosphere and a vacuum atmosphere to determine the best method for reducing pore size. Through the study, it was found that sintering in argon was more effective for pore size distribution and pore morphology when it was within a reasonable isothermal period. However, there were still some disadvantages to the method, such as having smaller pores but a higher density of pores when compared to VS.[13] Overall, both methods are effective with their respective limitations.

The material printed was the common high-performance aerospace alloy Ti-6Al-4V (Ti64). It combines a low density with high mechanical strength, making it a unique option within the metals space. Ti64 also has a high cost, therefore making AM an area of interest for making parts out of it. The standard AMS4999[1] outlined the goals for the mechanical properties of parts produced. This standard requires a minimum ultimate tensile strength (UTS) of 889 MPa, a yield strength of 799 MPa, and 6% elongation at failure. AMS4999 is a direct energy deposition standard, which is a beam-based process and makes it a good comparison for non-beam AM processes because it is made with an assumption of the inherent porosity of AM processes. This standard differs only slightly from the ASTM standard for wrought Ti64 in UTS and yield strength but provides a much lower percent elongation at failure to compensate for the increased porosity. Therefore, the goal of the group was to find a process that could create a sample that meets each of these goals.

3. Methods

3.1 Tensile Testing

The team used tensile testing to determine the strength of Ti-6Al-4V. The printability of the Ti64 allowed for a cylindrical tensile test specimen to be printed. However, due to a lack of grips that fit the geometry of that specimen, the team opted to test smaller test specimens that were cut out from a larger sample through electron discharge machining (EDM). The team pulled these smaller specimens on a Phenom XL SEM DEBEN Microtest Module. The team also employed digital image correlation (DIC) to calculate the strain in the material.

In total, the team received five hydrogen-processed samples and four VS samples with dimensions of approximately 6 mm in length, a 1-mm gauge width, and a 0.5-mm gauge thickness. To prepare the samples for DIC, the team polished the samples with 180-, 320-, and 600-grit sandpaper while lubricating them with water. After polishing, the samples were sprayed with a speckle pattern using an airbrush. To achieve this, the team used a 20 to 1 ratio of white paint to black printer toner by weight. The speckle pattern was applied in a single layer to achieve full coverage of the gauge and ensure an accurate DIC strain reading. Figure 3 shows a visual representation of a sample within the tensile testing setup. Immediately following the patterning, the samples were ready for tensile testing.

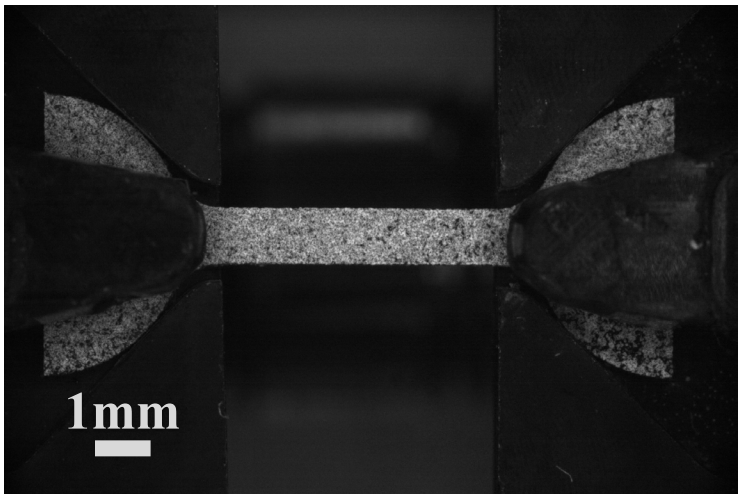

Fig. 3 VS Sample 2 with speckle pattern in the tensile test setup

The team used the DEBEN Microtest Module to pull the samples. The module was positioned beneath a camera, which recorded the entirety of the test. Point Grey FlyCapture software controlled the camera and its settings. More specifically, the team set the polarity to a maximum and determined the shutter speed by trial and

error. This ensured that as the samples were pulled, new material emerging to the surface did not disrupt the speckle pattern and ruin any DIC calculations.

The tensile test setup used tool steel grips to pull the samples. The team used a strain rate of 0.30-mm/s strain rate because it was the slowest strain rate available on the DEBEN system. The samples were pulled to failure.

Vic-2D computed the strain readings from the footage captured in tensile testing. Lagrangian strain in the X-direction was selected for strain maps, while a digital extensometer was used to compute the strain used for the stress–strain curves. The DIC strain readings were assumed to be more accurate than the strains from the displacement of the DEBEN module.

3.2 Hardness Testing

Hardness testing was performed to estimate the strength of the material. The type of hardness used on Fig. 4 is Vickers hardness with a load of 300 g. Each sample was indented 10 times. The goal was to achieve a hardness correlating to the UTS standards of AMS4999,[1] which dictate 889 MPa.

Fig. 4 Vickers hardness measurement system in the Zachry Lab

3.3 Archimedes Density Measurement

The Archimedes method determines the density of a part by using the Archimedes principle of buoyancy and multiple mass measurements. First, a sample is measured dry, in air, and then while submerged in water using a modified scale for these purposes. This second mass will be lower than the first due to the buoyant force. The volume of the water displaced by the part can then be calculated according to Eq. 1:

$$V = \frac{m_d - m_s}{\rho_w} \quad (1)$$

where V is volume, m_d is dry mass, $m_s$is submerged mass, and ρ_w is the density of water. The density is then calculated as the dry mass divided by the volume.

4. Results and Discussion

4.1 SEM Imaging

Scanning electron microscopy (SEM) images of Ti-6Al-4V were obtained for hydrogen-processed and VS microstructures (Figs. 5 and 6). In addition, energy-dispersive X-ray spectroscopy (EDS) was performed on the specimens to confirm their relative aluminum (Al)-vanadium (V) composition as well as analyze the composition of each phase. Tables 1 and 2 provide the data for Figs. 5 and 6, respectively.

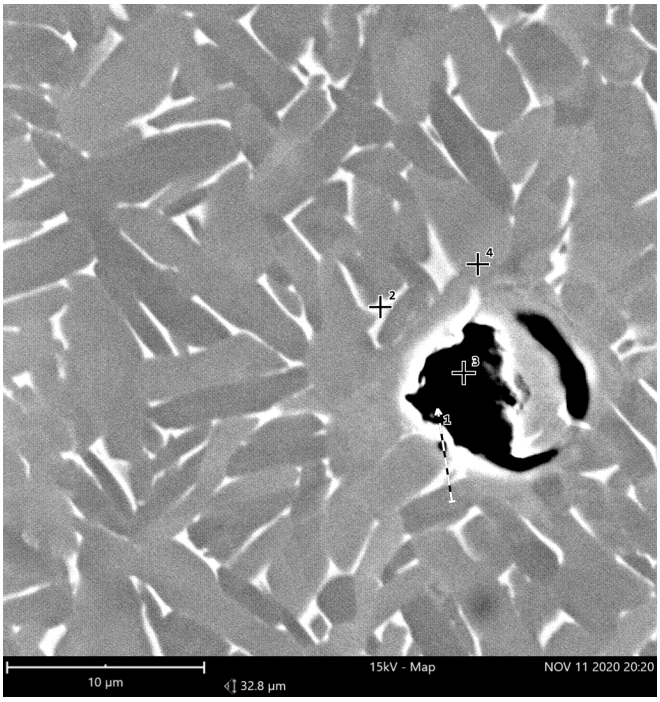

Fig. 5 VS- and THRM-processed EDS examination

Table 1 VS sample EDS data

VS	Element	Concentration (wt%)
Linescan 1	Ti	88.65
	Al	5.54
	V	5.81
Spot 2	Ti	76.88
	V	19.68
	Al	3.44
Spot 3	Ti	98.56
	Al	1.44
Spot 4	Ti	92.25
	Al	7.75

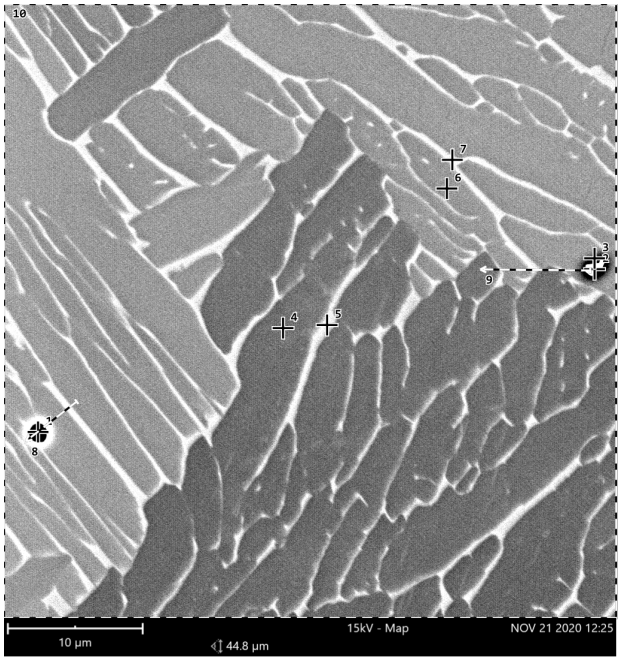

Fig. 6 VS microstructure and EDS

Table 2 VS EDS data

VS	Element	Concentration (wt%)
Linescan 9	Ti	87.62
	Al	6.68
	V	3.69
	Zinc (impurity)	2.01
Spot 4	Ti	90.79
	Al	7.59
	V	1.62
Spot 5	Ti	84.27
	Al	4.14
	V	11.59
Spot 6	Ti	90.45
	Al	7.54
	V	2.01

EDS data demonstrate conformity with typical Ti-6Al-4V microstructure. The line scans reveal a typical 6:4 Al-to-V relationship, accounting for some error resulting from crossing over different phase compositions. Spot analysis along the grain boundaries—such as Spot 2 in the hydrogen-processed sample and Spot 5 in the VS sample—reveal areas of strong V concentration, indicating a clear alpha-beta structure. The strong V concentration in the beta phase is compensated by slightly less than 4% V concentration in the primary alpha phase, as shown in Spot 4 in Fig. 6.

The immediate structural observation from the backscatter SEM images of Figs. 5 and 6 is that the HSPT microstructure appears to exhibit greater isotropy than the VS microstructure. This is supported by the obvious alignment of the V-rich phase in Fig. 6, as well as the nonuniformity in image intensity, which indicates a heterogeneous texture. These observations are consistent with observations that VS produces a much coarser microstructure in Ti-6Al-4V than the novel hydrogen sintering processes.[12] These results are also observed in the large-scale images in Figs. 7 and 8, which were compiled from individual tile images for each processing method.

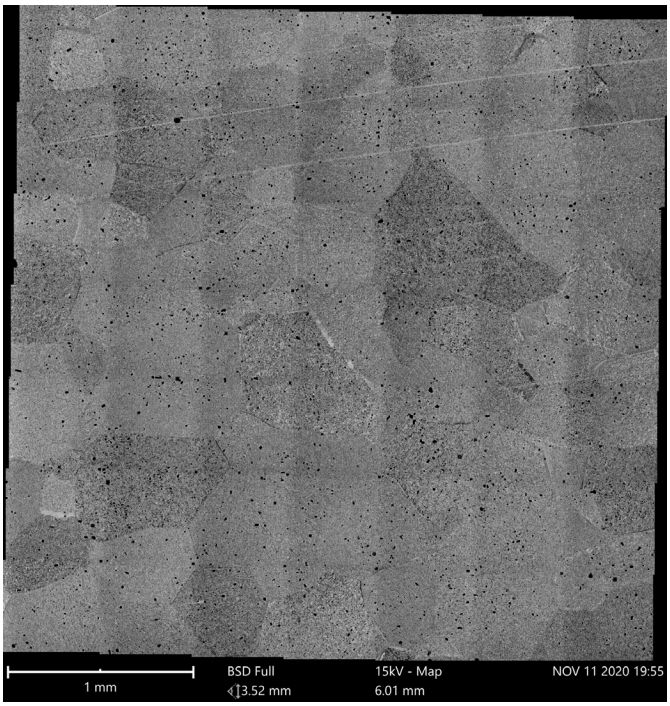

Fig. 7 Hydrogen-processed large-scale microstructure

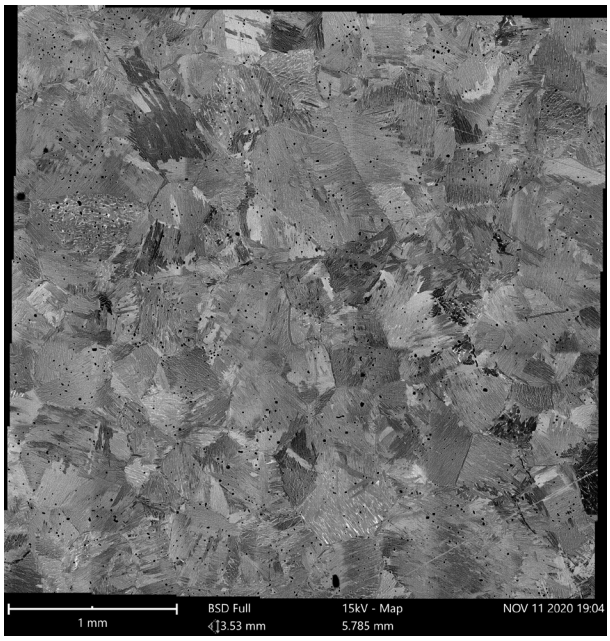

Fig. 8 VS large-scale microstructure

4.2 Hardness Testing

Table 3 compares two types of BJAM samples. As expected, the cold isostatic press (CIP) sample has a higher average compared to the as-received (AR) sample due to the CIP powder being more compacted than the AR. Both samples are porous;

however, AR is more porous and it was difficult to avoid pores when performing hardness tests. The BJAM sample is not the ideal candidate for the process because the high hardness would lead to a high approximated tensile strength. The samples have very high porosity; therefore, the BJAM sample is not suitable for the process as it would have a low real yield strength.

Table 3 BJAM samples: CIP and AR

Sample	CIP	AR
Average	443.17	391.4
Standard Deviation	37.94	56.69
Image	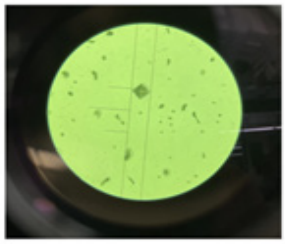	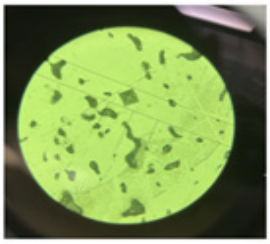

4.3 Archimedes Density Measurements

As seen in Table 4, the MEAM parts had relative densities of over 98% based on a theoretical density of 4.43 g/cm^3. This indicates that such parts should not have a detrimental level of porosity.

Table 4 Archimedes density measurements of the MEAM samples

Sample	Archimedes density (g/cm^3)	Relative density
Hydrogen processed	4.358	98.38%
VS (AR)	4.344	98.07%

4.4 Tensile Testing

Figure 9 shows the tensile testing data for the THRM Ti-6Al-4V samples. As previously mentioned, these tensile testing samples were miniaturized versions. In Fig. 9, Sample 2 fails earlier than the rest. The reason for this early failure is the result of the sample slipping during testing, and as such, the data point should be considered an outlier. Due to a lack of sample tests, the team decided to include the recorded data. Table 5 provides a summary of the tensile tests. The maximum stress value was used throughout the data to calculate the UTS of each sample. The Young's modulus was calculated from a linear fit of the elastic region of each sample; the slope of the curve was taken and then converted to units of gigapascals.

The Tabor relationship was utilized to approximate the hardness from yield strength values to provide a comparison to other measurements.

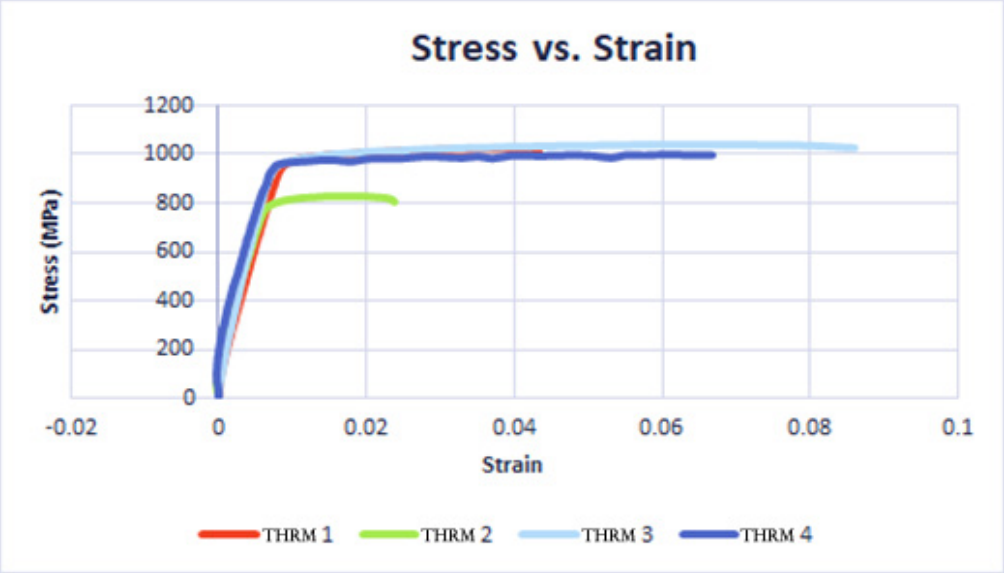

Fig. 9 Stress vs. strain curves for THRM samples of Ti-6Al-4V

Table 5 Data from stress vs. strain curves of THRM Ti-6Al-4V samples

Property	THRM 1	THRM 2*	THRM 3	THRM 4	Average
UTS (MPa)	1027	826	1037	1003	973
Young's modulus (GPa)	107.478	110.223	123.303	117.537	114.635
Stress at failure (MPa)	1022	818	1036	1003	970
Yield strength (MPa)	978	790	982	969	930
Hardness estimation (MPa)	326	263.33	327.33	323	310
% Elongation	4.5	2.4	8.7	7.0	5.65

* Sample deformed in grips and fractured outside of gauge, resulting in an invalid test.

As can be seen from both Fig. 9 and Table 5, all the samples performed similarly. When comparing these results to our goal of 889 MPa for the UTS, 799 MPa for the yield strength, and a 6% elongation, the THRM samples were able to meet or exceed these requirements. While there are a few discrepancies for THRM Sample 2, it can still be seen that all the other samples, which did not slip, were able to meet those goals.

Figure 10 shows the stress vs. strain curves for the VS Ti-6Al-4V samples. When paying close attention to Fig. 10, it can be seen that both samples have very similar moduli, yield strengths, and failure stresses. However, these samples did fail earlier than expected at about 2.4% and 3.6%—significantly smaller values than the THRM Ti-6Al-4V samples. Per the data in Table 6, the VS samples did not meet our goals. The UTS is approximately 200 MPa lower than we would like and the

yield strength is approximately 100 MPa lower. The hardness estimation of these samples was calculated in the same way as the THRM samples, where the yield strength was just divided by 3. While these values are still high, they are not as high those for the THRM samples, as seen in Tables 5 and 6.

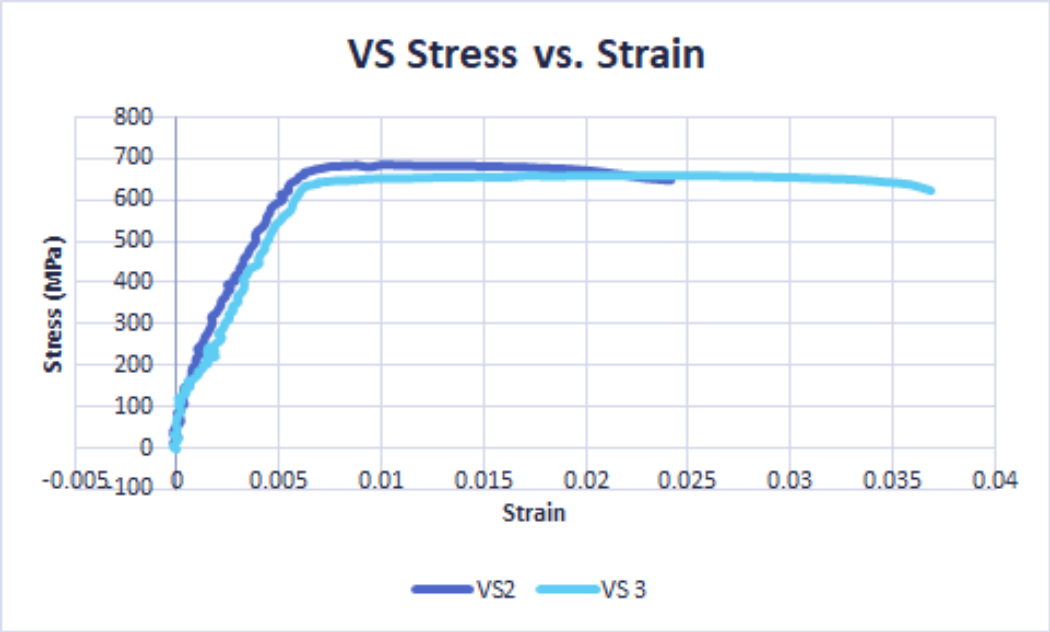

Fig. 10 Stress vs. strain curves for VS samples of Ti-6Al-4V

Table 6 Data from stress vs. strain curves of VS Ti-6Al-4V samples

Property	VS 2	VS 3	Average
UTS (MPa)	684	660	672
Young's modulus (GPa)	102.333	92.459	97.396
Stress at failure (MPa)	669	639	654
Yield strength (MPa)	683	649	666
Hardness estimation (MPa)	227.67	216.33	222
% Elongation (%)	2.4	3.6	3

As mentioned earlier, there was a total of five THRM samples and four VS samples. However, measurement errors resulted in no data collection for some of the samples. Overall, it can be concluded through Figs. 9 and 10 and Tables 5 and 6 that the best processing choice for AM is THRM, because it resulted in a UTS over 889 MPa, a yield strength over 799 MPa, and an elongation higher than 6%.

5. Conclusions

The BJAM process was eliminated due to the unmanageable level of inherent porosity in the parts. While this leads to high hardness values, these values would not properly convert to a high UTS due to these pores. Though, there is potential in the CIP sample, which had considerably lower porosity than the AR BJAM sample.

The MEAM samples were able to have tensile bars cut, and testing showed that the THRM method was superior to the VS method. This is due to the refinement in the microstructures that the THRM process allows for with the formation of the titanium hydride grains. The process reached the goals laid out by AMS4999[1] except for the percent elongation at failure. The average elongation value of 5.65% is below the goal of 6%, but this method could be further optimized to remove more pores.

The thermal profiles for THRM, HSPT, and the posttreatment process used to globularize or create bimodal microstructures[14] are shown in Fig. 11. THRM, as shown in Fig. 11a, is performed on a bulk, fully consolidated component. Since the material is already fully dense, the high-temperature portion of the curve is utilized to charge the material with hydrogen to the equilibrium concentration so that the grain-refining phase transformations can be performed with hydrogen as a temporary alloy addition. After grain refinement, the material is fully dehydrogenated in vacuum at a slightly elevated temperature. HSPT of MEAM and BJAM materials, as shown in Fig. 11b, requires an additional low-temperature stage to thermally debind the material before sintering in a hydrogen atmosphere at elevated temperature. The phase transformation and hydrogen removal steps are similar to THRM processing, but the exact procedure can vary depending on the geometry of the material and the desired microstructure. The highly refined microstructure produced by THRM and HSPT processing may be further modified using conventional heat treatments that have been established for wrought processed Ti-6Al-4V materials,[15] as shown in Fig. 11c. The treatment begins by heating the material to a temperature below the beta transus temperature, thereby increasing the overall fraction of beta phase in the material. At this point, the material can be furnace cooled to create more equiaxed alpha grains (i.e., globularization) or quenched to produce a bimodal microstructure. Aging at moderate temperatures can induce the formation of coherent ordered alpha (α_2) particles, which can improve the overall strength of the material.[16]

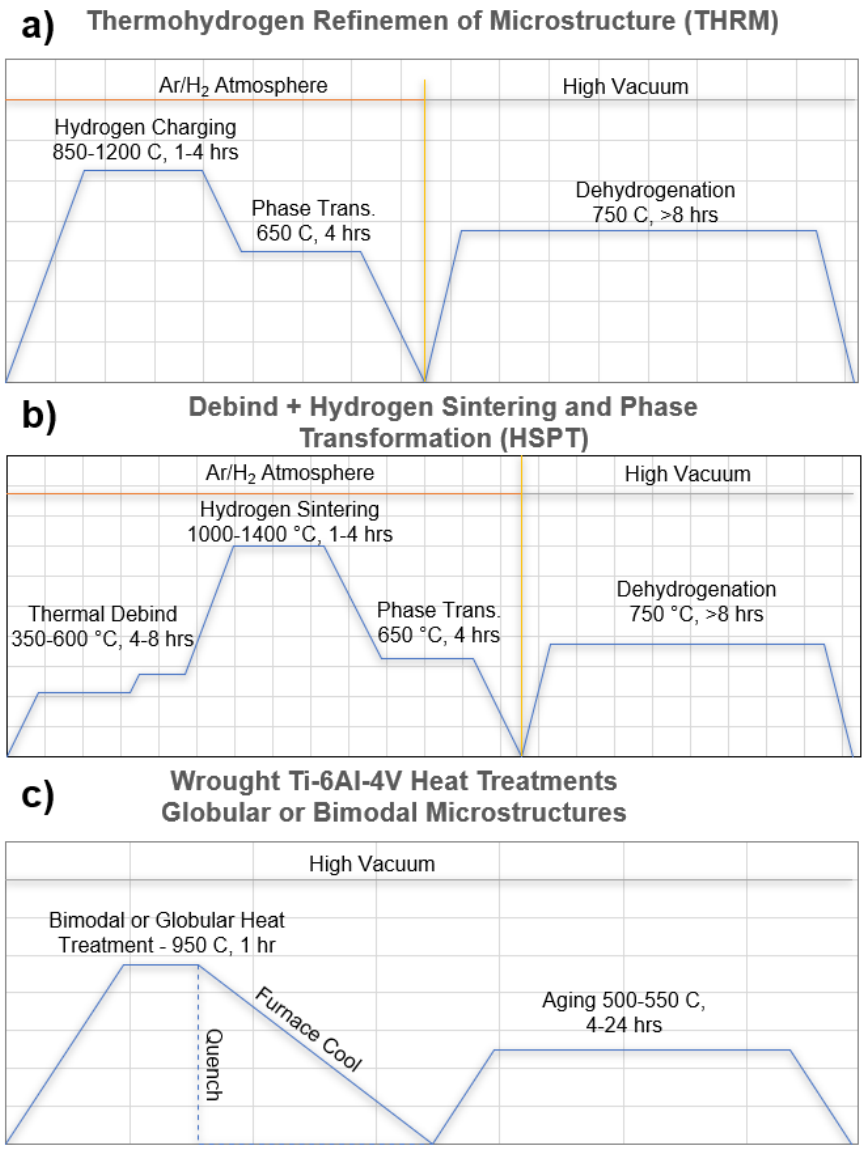

Fig. 11 Thermal treatments used throughout this project. a) THRM processed used to refine microstructure in bulk, fully consolidated Ti alloy components. THRM was used to improve the microstructure of conventionally sintered MEAM components. b) Debind and HSPT treatment for sintering and refining microstructure of fully sintered MEAM components. c) Optional heat treatment used for creating globularized and bimodal microstructures in wrought processed Ti.[18]

6. Recommendations

There are two areas that can be further studied and improved: 1) minimizing density by investigating the effects of powder packing and 2) maximizing the final strength by modifying the THRM profile.

The densities of the THRM parts were all above 98% of the relative density, but there is still some porosity that could lead to premature part failures, especially for large pores that could lead to significant stress concentrations. One way to minimize these porosities is to investigate and optimize the properties of the powder feedstocks. A wide range of powder sizes is desirable so that smaller particles can pack into the interstices of the larger particles. This, combined with normalized spherical power shapes, would allow for better green part densities, which will lead to a higher density in the final sintered parts. Overall, this recommendation will lead the parts to have a higher ductility.

Further exploration of the process could also be performed to better understand the relationship between the variables of THRM time and temperature on the refinement of the microstructure. The way this microstructure forms will greatly affect the mechanical properties of the produced parts. Another set of experiments could determine if there is any relationship between how the part is dehydrogenated, the time and temperatures, and the mechanical properties of the part, especially to determine if there are any annealing effects that are weakening the parts. A better understanding of the initial feedstock powder and treatment profiles will allow for further optimization of this designed AM process.

These steps have a strong potential for improving the mechanical properties of the parts, ensuring higher consistency in surpassing the requirements of AMS4999.[1]

7. References

1. AMS4999A. Titanium alloy direct deposited products 6Al - 4V annealed. SAE International; 2016 Sep 26.

2. Tuncer N, Bose A. Solid-state metal additive manufacturing: a review. 2020 Sep;72(9):3090–3111. doi: 10.1007/s11837-020-04260-y.

3. Vaezi M, Drescher P, Seitz H. Beamless metal additive manufacturing. 2020;13(4). doi: 10.3390/ma13040922.

4. Ziaee M, Crane NB. Binder jetting: a review of process, materials, and methods. Addit Manuf. 2019 Aug;28:781–801.

5. Mostafaei A, Rodriguez De Vecchis P, Nettleship I, Chmielus M. Effect of powder size distribution on densification and microstructural evolution of binder-jet 3D-printed alloy 625. Mater Des. 2019;162:375–383. doi: https://doi-org.srv-proxy2.library.tamu.edu/10.1016/j.matdes.2018.11.051.

6. Bai Y, Williams CB. The effect of inkjetted nanoparticles on metal part properties in binder jetting additive manufacturing. Nanotechnology. 2018;29(39):395706. doi: 10.1088/1361-6528/aad0bb.

7. Ziaee M, Tridas EM, Crane NB. Binder-jet printing of fine stainless steel powder with varied final density. JOM. 2017;69(3):592. doi: 10.1007/s11837-016-2177-6.

8. Srivastava M, Rathee S, Maheshwari S, Kundra TK. Additive manufacturing: fundamentals and advancements. Milton: Taylor & Francis Group; 2019. http://ebookcentral.proquest.com/lib/tamucs/detail.action?docID=5896935.

9. Gong H, Snelling D, Kardel K, Carrano A. Comparison of stainless steel 316L parts made by FDM- and SLM-based additive manufacturing processes. JOM. 2019;71(3):880. doi: 10.1007/s11837-018-3207-3.

10. Annoni M, Giberti H, Strano M. Feasibility study of an extrusion-based direct metal additive manufacturing technique. Procedia Manufacturing. 2016;5:916–927. doi: 10.1016/j.promfg.2016.08.079.

11. Gibson I, Rosen D, Stucker B. Powder bed fusion processes. Additive manufacturing technologies. Springer Science+Business Media; 2015. ch. 5; sec. 3.1; p. 112.

12. Sun P, Fang ZZ, Koopman M, Xia Y, Paramore J, Ravi Chandran KS, Ren Y, Lu J. Phase transformations and formation of ultra-fine microstructure during

hydrogen sintering and phase transformation (HSPT) processing of Ti-6Al-4V. Metall Mater Trans A. 2015;46:5546–5560. doi: 10.1007/s11661-015-3141-8.

13. Luo SD, Liu B, Tian J, Qian M. Sintering of titanium in argon and vacuum: pore evolution and mechanical properties. Int J Refract Metals Hard Mater. 2020;90:105226. doi: 10.1016/j.ijrmhm.2020.105226.

14. Paramore JD, Fang ZZ, Dunstan M, Sun P, Butler BG. Hydrogen-enabled microstructure and fatigue strength engineering of titanium alloys. Sci Rep. 2017. doi.org/10.1038/srep41444.

15. Boyer R, Welsch G, Collings EW. Materials properties handbook: titanium alloys. 2nd ed. ASM International; 1998.

16. Lutjering G, Williams J. Titanium. 2nd ed. Springer Berlin Heidelberg; 2007. doi.org/10.1007/978-3-540-73036-1.

List of Symbols, Abbreviations, and Acronyms

3-D	three-dimensional
Al	aluminum
AM	additive manufacturing
AR	as-received
ARL	Army Research Laboratory
ASTM	American Society for Testing and Materials
BJAM	binder jetting additive manufacturing
CIP	cold isostatic press
DEVCOM	US Army Combat Capabilities Development Command
DIC	digital image correlation
EDM	electron discharge machining
EDS	energy-dispersive X-ray spectroscopy
HSPT	hydrogen sintering and phase transformation
MEAM	metal extrusion additive manufacturing
SEM	scanning electron microscopy
SLM	selective laser melting
THRM	thermohydrogen refinement of microstructure
Ti	titanium
UTS	ultimate tensile strength
V	vanadium
VS	vacuum sintering

1 (PDF)	DEFENSE TECHNICAL INFORMATION CTR DTIC OCA
1 (PDF)	DEVCOM ARL FCDD RLD DCI TECH LIB
2 (PDF)	DEVCOM ARL FCDD RLW MF BG BUTLER JD PARAMORE